A Proxy for High-Resolution Regional Reanalysis for the Southeast United States: Assessment of Precipitation Variability in Dynamically Downscaled Reanalyses

Lydia Stefanova[1], Vasubandhu Misra[1,2], Steven Chan[1,3,4], Melissa Griffin[1], James J. O'Brien[1] and Thomas J. Smith III[5]

[1] Center for Ocean-Atmospheric Prediction Studies (COAPS), The Florida State University, Tallahassee, FL, USA

[2] Department of Earth, Ocean and Atmospheric Science, The Florida State University, Tallahassee, FL, USA

[3] School of Civil Engineering and Geosciences, Newcastle University, Newcastle-upon-Tyne, UK

[4] Met Office Hadley Centre, Exeter, UK

[5] Southeast Ecological Science Center, U.S. Geological Survey (USGS), St. Petersburg, FL, USA

Abstract

We present an analysis of the seasonal, subseasonal, and diurnal variability of rainfall from COAPS Land-Atmosphere Regional Reanalysis for the Southeast at 10-km resolution (CLARReS10). Most of our assessment focuses on the representation of summertime subseasonal and diurnal variability. Summer precipitation in the Southeast United States is a particularly challenging modeling problem because of the variety of regional-scale phenomena, such as sea breeze, thunderstorms and squall lines, which are not adequately resolved in coarse atmospheric reanalyses but contribute significantly to the hydrological budget over the region.

We find that the dynamically downscaled reanalyses are in good agreement with station and gridded observations in terms of both the relative seasonal distribution and the diurnal structure of precipitation, although total precipitation amounts tend to be systematically overestimated. The diurnal cycle of summer precipitation in the downscaled reanalyses is in very good agreement with station observations and a clear improvement both over their "parent" reanalyses and over newer-generation reanalyses. The seasonal cycle of precipitation is particularly well simulated in the Florida; this we attribute to the ability of the regional model to provide a more accurate representation of the spatial and temporal structure of finer-scale phenomena such as fronts and sea breezes. Over the northern portion of the domain summer precipitation in the downscaled reanalyses remains, as in the "parent" reanalyses, overestimated.

Given the degree of success that dynamical downscaling of reanalyses demonstrates in the simulation of the characteristics of regional precipitation, its favorable comparison to conventional newer-generation reanalyses and its cost-effectiveness, we conclude that for the Southeast United states such downscaling is a viable proxy for high-resolution conventional reanalysis.

1. Introduction

The scientific community involved with the hydrological, ecological and biological modeling of the Earth system is showing a growing demand for reliable high-resolution meteorological data sets that provide fine spatial and temporal detail of near-surface variables (e.g Clark et al 2001, Rahbek and Graves 2001, Shukla et al 2009). A conventional global or regional reanalysis is very resource-intensive. Furthermore, the degree to which the assimilation of observations, such as radiosondes, which are sparse in space and time – there are about 90 upper air observation stations over North America, taking measurements once or twice each day (http://www.ua.nws.noaa.gov/) – would be beneficial when reanalysis grids are approaching 10-km or higher resolutions is unclear.

This paper is devoted to examining the seasonal and boreal summer diurnal variability of precipitation in two regionally downscaled dynamical model integrations over the Southeast United States. The Southeast United States are of particular interest for such downscaling, given the large proportion of agricultural lands, endangered habitats, and large cities with water management concerns in the region. Precipitation, especially of convective nature, is one of the most challenging variables for any reanalysis. A high-resolution model is a necessary prerequisite for the accurate representation of convective precipitation in a region with complex coastal geometry.

The present work is motivated by a similar kind of model integration over California (Kanamitsu and Kanamaru 2007; Kanamaru and Kanamitsu 2007b), wherein it was shown that high-resolution downscaling from a coarse-resolution reanalysis produces regional features that are in encouraging agreement with station observations. Such dynamical downscaling is made viable by assuming that small scales are governed by the large-scale forcing and any feedback from the small to the large scales is insignificant. In fact, Kanamaru and Kanamitsu (2007b) showed that a regional model with high spatial resolution forced at the lateral boundaries by a realistic large-scale forcing is capable of generating features that are comparable, and in some instances an improvement, to the much more resource-intensive North American Regional Reanalysis (NARR; Mesinger et al. 2006). Von Storch et al. (2000) claimed that such dynamical downscaling analysis from a coarser reanalysis may be considered "a poor person's data assimilation technique", since it doesn't require the direct assimilation of observations.

There has been a growing recognition that nudging the state variables toward the large-scale forcing can significantly reduce regional climate model drift in the interior of the regional domain (von Storch et al. 2000; Castro et al. 2005; Kanamaru and Kanamitsu 2007a). As a result, the large-scale analyses, such as the NCEP-NCAR reanalysis (Kalnay et al. 1996), the NCEP-DOE reanalysis II (hereafter R2; Kanamitsu et al. 2002) or the ECMWF's ERA40 (hereafter ERA40; Uppala et al. 2006), can be downscaled continuously in time for the period of the available reanalysis without periodically reinitializing the regional model. This continuous dynamic downscaling from reanalysis is far less expensive than conventional data assimilation and provides meteorological data sets that are self-consistent (i.e., whose energy and water budgets are completely accountable; Kanamitsu and Kanamaru 2007).

Seasonal forecasts for the summer season in the Southeast United States present a significant challenge. Many of the seasonal prediction models exhibit extremely poor skill in precipitation and surface temperature forecasts over the region (Stefanova et al. 2011). A high-resolution model is essential in capturing the spatial and temporal distribution of rainfall in the region. Lim et al. (2010) showed that the downscaling of R2 with RSM at 20 km over the Southeast results in a reduced wet bias and a more realistic spatial pattern of summer precipitation, with improved spatial and temporal (interannual) correlation and reduced mean square error of summer rainfall totals. While Lim et al. (2010) was limited to summer precipitation totals from separate summertime initializations of the regional model, here we present a detailed analysis of the seasonal, subseasonal, and diurnal variability of rainfall from a continuous twenty-two-year-long integration that we call the COAPS Land-Atmosphere Regional Reanalysis for the Southeast at 10-km resolution (hereafter CLARReS10). The global reanalyses, R2 (with a native grid resolution of approximately 1.875 degrees latitude and longitude) and ERA40 (with a native grid resolution of approximately 1.1 degrees latitude and longitude), have been dynamically downscaled with the RSM, resulting, respectively, in the CLARReS10-R2 and CLARReS10-ERA40 data sets. The downscaling has been performed over the Southeast United States at a horizontal resolution of 10 km and is continuous for the period 1979–2001. The two downscaled reanalyses are compared to gridded observations and station data. Specifically, this paper analyzes the ability of such continuous dynamical downscaling over the Southeast United States to create a realistic temporal structure of precipitation. In addition to addressing the average annual cycle, the paper focuses on the summertime precipitation variability. The summer season in the Southeast United States supports a variety of pertinent small-scale features (such as sea breeze, thunderstorms, squall lines, tropical and extratropical cyclones) that are not adequately resolved in many of the existing atmospheric reanalyses.

These phenomena do, however, contribute significantly to the hydrological budget over the region (e.g. Winsberg 2003; Misra et al. 2011).

The remainder of this paper is structured as follows: section 2 provides details about the regional model, domain, and initial and boundary conditions; section 3 describes the validation data sets; section 4 presents the study results; and finally, section 5 briefly summarizes the study findings.

2. Model description and forcing

This study uses the RSM model originally developed at NCEP (Juang and Kanamitsu 1994) and now maintained at the Experimental Climate Prediction Center at the University of California at San Diego (UCSD) (Kanamitsu and Kanamaru 2007). An attractive feature of the RSM is the scale-selective bias correction (SSBC). It allows the downscaling (or nesting) ratio to be much greater than 1:3 (used typically in other regional models; Warner et al 1997); Kanamaru and Kanamitsu (2007a) show that SSBC makes the solution from the RSM relatively insensitive to the size of the regional domain and the location of the lateral boundaries. In independent regional modeling studies with other regional climate models, it has been shown that spectral nudging of the smallest wave numbers (or largest wavelengths of the regional domain) toward the large-scale forcing is necessary to avoid unrealistic regional climate model drift (von Storch et al. 2000; Castro et al. 2005).

The regional model domain extends from 24^{o}N to 36^{o}N and from 90^{o}W to 76^{o}W (Fig. 1). RSM uses the winds, temperature, humidity, and surface pressure of the global reanalyses (either R2 or ERA40) at six-hourly intervals as lateral boundary conditions. In the interior of the domain, RSM uses SSBC with a damping scale of 1000 km, which nudges the large-scale features within the regional domain toward the global reanalysis. The nudging is performed uniformly at all vertical levels. The RSM model configuration used here is shown in Table 1. For this study, the most important change to the RSM version used by Kanamitsu and Kanamaru (2007b) and Kanamaru and Kanamitsu (2007) is the replacement of the Oregon State University land surface scheme (Pan and Mahrt 1987) with the more recently developed NOAH land surface scheme (Ek et al. 2003). The sea surface temperatures for these integrations are from the National Oceanic and Atmospheric Administration (NOAA) Extended Reconstruction Sea Surface Temperature analysis version 3 (ERSSTV3; Smith et al. 2008). The model deep convection is parameterized using the simplified Arakawa-Schubert scheme (SAS; Pan and Wu 1995), and shallow convection is parameterized following Slingo (1987).

3. Validation data sets

We use the following observational station and gridded data sets for model validation:

a) Monthly: PRISM gridded precipitation at 4-km resolution (Daly et al. 1994) and National Climate Data Center (NCDC) monthly station climatology for the period 1971–2000 available online from http://www.ncdc.noaa.gov/oa/documentlibrary/pdf/eis/clim20eis.pdf

b) Daily: NOAA Climate Prediction Center (CPC) Daily US Unified Precipitation at 0.25° (1979–1998) (Higgins et al. 1996)

c) Hourly: Automated Surface Observing Stations (ASOS) and Automated Weather Observing Stations (AWOS) observations from NCDC (http://www.ncdc.noaa.gov/oa/climate/stationlocator.html). We also use two additional data sets of remotely sensed precipitation observations with limited temporal coverage: the Tropical Rainfall Measurement Mission (TRMM) 3B42 3-hourly multi-satellite precipitation analysis (Huffman et al 2007), available since 1998 at a 0.25 degree resolution, and the NCEP/ Environmental Modeling Center (EMC) US gridded multi-sensor estimated hourly precipitation analysis at 4 km for the period 2004-2009 (Lin and Mitchel 2005).

Additionally, we use the hourly precipitation from two new-generation reanalyses—NCEP's Climate Forecast System Reanalysis (CFSR; Saha et al. 2010) and NASA's Modern Era Retrospective Analysis for Research and Applications (MERRA; Bosilovich et al. 2008) for comparison of the diurnal cycle of summer precipitation.

4. Results

4.1 Seasonal cycle

The seasonal cycle was calculated over nine broad subregions (north and south Alabama and Georgia, South Carolina, the western and eastern Florida Panhandle, and central and south Florida; red boxes in Fig. 1). The regions were selected to be of equal size (3°-by-2°) and roughly fit within the geographical state boundaries. The average precipitation of each calendar month is divided by the average annual total precipitation (Fig. 2; note the wet bias in both CLARReS10-R2 and CLARReS10-ERA40) to give each month's fractional contribution to the annual average (Fig. 3). Here the observed values (PRISM, black dashed line) are compared to the global reanalyses (R2, blue dots; ERA40, red dots) and to the corresponding regional reanalyses (CLARReS10-R2, blue line; CLARReS10-ERA40, red line).

In the majority of the subregions the observations indicate a primary annual peak of rainfall in the boreal summer preceded by a secondary peak in the boreal spring months. North Alabama is the only subregion without an observed summer precipitation peak. In south Alabama and north Georgia the summer peak is present but secondary to the spring peak, and in south Florida the spring peak is nearly absent. Overall, the large-scale reanalyses have a tendency to underestimate the contribution of the spring precipitation peak to the annual total and to overestimate the contribution of the summer precipitation peak. In the majority of subregions the benefit of downscaling is a reduction of this bias. In both CLARReS10-R2 and CLARReS10-ERA40 the relative dry bias in the spring months is reduced (especially in north Florida and south Alabama). In the summer months the CLARReS10 data sets reduce the wet biases of their respective global reanalyses.

For both the spring and summer seasons, the amount of bias reduction is larger for the downscaling of R2 compared to the downscaling of ERA40 (not because the downscaled R2 is much closer to observations than the downscaled ERA40, but rather because the global R2 is further away to begin with). However, both the global and regional reanalyses incorrectly generate a summer precipitation maximum over north Alabama and overestimate the summer maxima for north Georgia and south Alabama, and, to a lesser extent, those for South Carolina and south Georgia. Over Florida, however, the seasonal cycle of the regional reanalyses matches well with observations.

The regionally averaged results are similar to those obtained at individual stations (not shown): the global reanalyses tend to overestimate the contribution of summer precipitation to the annual total and to underestimate the contribution of the spring and winter precipitation. In contrast, both regionally downscaled reanalyses are relatively closer to the observations of the seasonal cycle of precipitation.

4.2 Phenomenological comparison of coarse and fine-resolution precipitation

The reduction of bias of the regional reanalyses compared to their "parent" global reanalyses is likely attributable to the regional model's ability to resolve the precipitation associated with finer-scale phenomena, such as frontal passages and sea breeze circulation while remaining constrained to the reanalyses at the synoptic and regional scale by the SSBC. For brevity, we restrict the following two demonstrations to a comparison between ERA40 to CLARReS10-ERA40; the comparison between R2 and CLARReS10-R2 is no different in nature. Fig 4 illustrates one such example, the passage through the region of a strong frontal system on March 13, 1993. This frontal system, dubbed "storm of the century", was a large cyclonic storm and was unique for its intensity with hurricane-strength winds, massive size and its wide reaching effect (Kocin et al. 1995). There were torrential rains in central Florida with measurable snowfall as far south as north Florida associated with this storm (Kocin et al 1995). In comparison with observations in Fig. 4f, the fine scale banded features of precipitation absent in ERA40 (Fig. 4a) is reasonably well captured by CLARReS10-ERA40 (Fig. 4b). The location and even the precipitation rates in Florida, Georgia, South Carolina, and Southern Alabama are very well captured in CLARReS10-ERA40. However the MSLP in ERA40 (Fig. 4a) and

CLARReS10-ERA40 (Fig. 4b) are comparable to each other with the lowest pressure around 985 hPa while observations (Fig. 4e) indicate the lowest pressure of 972 hPa centered at the border of Georgia and South Carolina. The convergence fields in Figs. 4c and d are quite consistent and reflective of the precipitation field of ERA40 and CLARReS10-ERA40 respectively. The fine scale features of convergence and their higher magnitudes in CLARReS10-ERA40 (Fig. 4d) are poorly resolved in ERA40 (Fig. 4c).

The sea breeze representation in the global and regional models is illustrated on the example of composite diurnal cycle for three consecutive summer days (28 July 2000 – 30 July 2000) from ERA40 (Fig 5), CLARReS-ERA40 (Fig. 6) and the Tropical Rainfall Measuring Mission (TRMM) 3B42 observations (Huffman et al 2007) (Fig 7). These days were randomly picked from the peak of the summer season and within the TRMM satellite's observing period and have not been selectively chosen beyond that. The composite surface convergence field of ERA40 (Fig 5) has much smaller magnitudes than that of CLARReS10-ERA40 (Fig. 6). In CLARReS10-ERA40 there is a pronounced pattern of diurnally varying convergence/divergence parallel to the coastline. By 18 GMT (2pm EDT), a convergence line forms on the inland side of the coast with a corresponding divergence line over the water. As time progresses to 00 GMT (8pm EDT), the convergence region broadens and spreads further inland, while the divergence broadens and spreads further over the water. The converse process takes place between 06 and 12 GMT (2 and 8am EDT) as the land-ocean temperature gradients switch sign, such that by 12 GMT (8am EDT) the convergence is over water and divergence is over land. This dramatic diurnal variation of low-level convergence is all but absent in ERA40. Although a direct validation of the diurnal variability of convergence is not possible due to lack of data, the behavior of CLARReS10-ERA40 is in agreement with the conceptual understanding of sea breeze circulation (e.g. Abbs and Physick 1992). The comparison of the convergence field with the 6-hourly accumulated precipitation is also in conceptual agreement with sea-breeze circulation. The largest 6-hourly mean precipitation rates in CLARReS10 (>32mm/day) are found over the areas of strongest surface convergence (South Florida at 00 GMT (8pm EDT) and the Florida/Georgia border at 18 GMT (2pm EDT)). These validate remarkably well with the TRMM 3B42 observations (Fig 7). ERA40, by contrast, has no precipitation rates exceeding 32 mm/day over Florida or Georgia, and its timing and spatial structure of the sea-breeze precipitation is incorrect.

4.3 Summer mean and variance

We next examine the reanalyses' climatological means and variances for the summer months, June, July and August (JJA) (Fig. 8). The well-known overall wet bias of R2 (Kanamitsu et al. 2002) is apparent (Fig. 8a), as is the more realistic mean JJA precipitation from ERA40 (Betts et al 2006) (Fig. 8b). CLARReS10 reduces the wet bias of R2 (Fig. 8c) but introduces a wet bias to ERA40 (Fig. 8d). This seeming contradiction can be explained by the difference in convective parameterization between the two global reanalyses, and by possible differences in the boundary conditions provided by the two reanalyses to the regional model. Since, as we will illustrate shortly, ERA40 contains more low-level moisture than R2, CLARReS10-ERA40 has more precipitation than CLARReS10-R2. However, despite the increased moisture in ERA40 compared to R2, the physics package for R2 produces larger precipitation amounts. In both regional downscalings the average summer precipitation rate is overestimated by about 2 to 3 mm/day (or approximately 6 to 9 cm/month). However, the local maxima in south Florida, western central Florida and the Florida Panhandle are present (if overestimated) in the CLARReS10 data sets.

The interannual variance of JJA mean rainfall as illustrated by the standard deviation shows that both R2 and ERA40 capture the high variance in the Florida Panhandle; however, R2 (unlike ERA40) underestimates the variance over southwest and central Florida. The magnitudes and geographical distribution of interannual variance of summer precipitation are simulated relatively well in the CLARReS10 data sets, with foci of variance around the central Florida Panhandle and the western coast of central Florida.

4.4 Summer precipitation frequency

Is the excess of precipitation in the downscaled reanalyses, particularly outside Florida, the result of an increased number of rainy days or an increased frequency of heavy precipitation events? To address this question, we calculated the average percentage of days (in JJA with precipitation exceeding thresholds of 0.5, 1, 5, 10, 15, 20, and 30 mm for the two global and their corresponding downscaled reanalyses and the CPC Daily US Unified Precipitation, and averages (over the boxes in Fig. 1) of the percentage of days in JJA exceeding a threshold of 0. The latter averages were calculated for the two global reanalyses, their corresponding downscaled reanalyses, and CPC Daily US Unified Precipitation (Fig. 9).

For all nine subregions of the domain, R2 overestimates the probability of precipitation exceeding any threshold. At the same time, the frequency of relatively light (<5 mm) precipitation days is somewhat underestimated. ERA40, on the other hand, overestimates the frequency of days with up to 10 mm of precipitation, and underestimates the frequency above that threshold. Averaged over the subregions, both CLARReS10 data sets are very close in terms of their probabilities of exceedance, with the exception of South Florida, where CLARReS10-ERA40 strongly overestimates the frequency of precipitation days at all thresholds above 5mm, while CLARReS10-R2 matches well with the observed frequencies. In the remainder of the domain, both CLARReS10 generally underestimate the frequency of days with light precipitation (<5mm), and slightly overestimate the frequency of days with precipitation greater than 5mm.

Outside Florida, both regional reanalyses overestimate the overall frequency of rainy days (daily precipitation exceeding 1 mm) by roughly 5 to 15 percentage points and the standard deviation of that frequency by up to 25 percentage points. CLARReS-R2, with its reduced frequency of rainy days outside Florida, conforms to the observations better than CLARReS10-ERA40 does. In most of Florida, this frequency is underestimated, particularly by CLARReS10-R2. In general, the average frequency of rainy days in summer is higher in the CLARReS10-ERA40 downscaling than in CLARReS10-R2.

Both in Florida and in the remainder of the domain, days with heavy (>20 mm) precipitation are also more frequent in CLARReS10-ERA40 compared to CLARReS10-R2. Over Florida both downscaled reanalyses demonstrate a pattern similar to observations in terms of the spatial distribution, with a broad maximum over peninsular Florida and the Gulf. The percentage of heavy precipitation days in Florida in CLARReS10-R2 is in very good agreement with the observations; however, in the southern part of the Florida peninsula, CLARReS10-ERA40 overestimates the frequency of heavy precipitation days by up to 25 percentage points. Outside Florida, heavy precipitation days are more frequent in the downscaled reanalyses than they are in observations, especially in CLARReS10-ERA40. Both regional reanalyses correctly identify a relatively high interannual variability of the number of heavy precipitation days in the Florida panhandle.

Comparison of the downscaled reanalyses with the corresponding observations (not shown) demonstrates that, not surprisingly, rainy days are generally more frequently observed in wet years than in dry years, and that this interannual variation of the frequency of rainy days is relatively well captured by both regional reanalyses, especially over peninsular Florida and east of the Appalachians.

What accounts for the drastic difference between the climatology of summer precipitation in the two downscaled reanalyses in South Florida seen in Figs 8 and 9? A Hovmüller diagram of the difference in precipitation between CLARReS10-ERA40 and CLARReS10-R2 at 25.5N (Fig 10a) demonstrates that the difference systematically manifests each summer, and therefore cannot be attributed to a limited number of extreme events. Although it is impossible to definitively identify the source of this difference it is likely a consequence of the increased low-level (1000-850mb) moisture convergence to the east (i.e., generally upstream) of the precipitation excess and increased low-level moisture (Fig 10b) and total column precipitable water (not shown) in CLARReS10-ERA40 compared to CLARReS10-R2. The difference in low-level moisture content can be traced back to the “parent” reanalyses (Fig. 11). The global ERA40 reanalysis generally contains more low-level moisture than R2 throughout the domain during the summer; this difference increases towards the southern part of peninsular Florida. It is likely that at least some of the discrepancy between the two reanalyses can be attributed to their different native resolutions (1.1 degrees for ERA40, 1.875

degrees for R2) and the consequent discrepancy in land-sea mask representation, and different formulations of convective precipitation, but pinpointing its exact source is beyond the scope of the present paper.

We selected two years, 1992 and 1994, to illustrate the consequences of having large (1992) vs. small (1994) difference of the low-level moisture fields between ERA40 and R2 over south Florida (see Fig. 10). When the JJA low-level moisture in ERA40 is larger than that in R2, as is the case for majority of years, the precipitation in CLARReS10-ERA40 far exceeds that in CLARReS10-R2 over south Florida (Fig. 12a). In the case when the low-level moisture in ERA40 is similar to that in R2, the precipitation amounts for south Florida in CLARReS10-ERA40 and CLARReS10-R2 are much closer (Fig. 12b). The observed difference in precipitation between the two years (Fig 12e, f) shows a wet anomaly extending from Florida's panhandle through southeastern Alabama and most of inland Georgia to western South and North Carolina. South Florida, northwestern Alabama, western Mississippi, Tennessee and the coastal areas of Georgia, North and South Carolina are dominated by a dry anomaly; of these, the largest anomaly values are found in south Florida. Both CLARReS10-R2 and CLARReS10-ERA40 capture the wet anomaly well, although both extend it further west than the observations. CLARReS10-R2 fails to represent the dry anomaly of south Florida (Fig. 12c); CLARReS10-ERA40 (Fig. 12d), on the other hand, captures it very well.

4.5 Diurnal cycle

The diurnal cycle of summer precipitation in the coastal regions of the Southeast United States is dominated by the sea breeze effects (Byers and Rodebush, 1948). The sea breeze circulation is set into motion by the land-ocean temperature gradient. Along the Florida peninsula, on average, the sea breeze peaks earlier at the east cost than at the west coast, and the timing of the peak increases going from south to north; maximum sea breeze thunderstorm activity is found in the southwest corner of the peninsula (Schwartz and Bosart 1979, Blanchard et al. 1985, Michaels et al. 1987).

The average time of diurnal summer rainfall maximum from CLARReS10-R2 and CLARReS-ERA40 (Fig. 13) illustrates the diurnal evolution of model convection. Along the coast, precipitation peaks in the late afternoon, between 20 and 22 GMT (4pm and 6pm EDT) in CLARReS10-R2 and generally about an hour or two earlier in CLARReS10-ERA40. Inland maxima are achieved in the early evening, between 22 and 24 GMT (6pm and 8pm EDT; CLARReS10-R2) and between 21 and 23 GMT (5pm and 7pm EDT; CLARReS10-ERA40). The difference between CLARReS10-R2 and CLARReS10-ERA40 is shown in Fig. 13, bottom left. Gridded hourly observations are not available for the period 1979-2001. Instead, we compare the timing of diurnal maximum of precipitation to that of the NCEP/ EMC US gridded multi-sensor estimated hourly precipitation analysis for the period 2004-2009 (Fig. 13, bottom right). A qualitative comparison between this analysis and the two CLARReS10 data sets, assuming that the interannual variability of the timing of precipitation maximum is negligible, suggests that the CLARReS10-ERA40 is better at representing the diurnal cycle of Florida, while CLARReS10-R2 is better at representing the diurnal cycle in the remainder of the domain.

The hourly evolution of the precipitation rate during an average summer day for several stations throughout the region (Fig. 14) illustrates the skill of the CLARReS10 data set in simulating the diurnal variability of rainfall. The results were also compared to the "parent" global reanalyses and to the CFSR and MERRA reanalyses. The summertime diurnal cycle in CLARReS10 is in very good agreement with station observations, particularly in Florida, and an improvement over both R2 and ERA40. Both CLARReS10-R2 and CLARReS10-ERA40 are also clearly superior to the new-generation global reanalyses, CFSR and MERRA. A likely explanation for the early rainfall maximum and overestimated precipitation amounts by CFSR is a possible bias in soil moisture and evapotranspiration during the wet season (Silva et al 2011).

5. Summary and conclusions

In this study we dynamically downscaled two large-scale global reanalyses to a high-resolution 10-km grid over the Southeast United States. The continuous downscaling was performed over two decades of data. The resulting two data sets, which we call CLARReS10, show significant improvement in their rendition of the means and variance of seasonal cycle and summer season rainfall over most of the Southeast United States, and especially over Florida, as evidenced by comparisons to gridded and station observations. This improvement can be attributed to the ability of the regional model to create a more accurate representation of the spatial and temporal structure of finer-scale phenomena, such as the precipitation associated with cold season frontal passages and warm season sea breeze circulations, while remaining constrained to the reanalyses at synoptic scales by SSBC. An accumulation of multiple better-resolved precipitation events would naturally result in an improved climatology.

Likewise, the simulation of the diurnal cycle of rainfall, particularly over Florida, is in very good agreement with station observations and a clear improvement over the coarser global reanalyses CFSR and MERRA. We believe that this is a consequence of the higher resolution of CLARReS10, which results in a better resolution of the coastline and land-ocean temperature contrast that can drive the mesoscale circulations associated with these gradients. In addition to CLARReS10 having a slightly higher resolution than MERRA and CFSR, all three reanalyses use different physics packages in their respective models. While we are not claiming superiority of the physics used in RSM, we believe that the scale-selective bias correction and higher resolution collectively contribute to the improvements seen in CLARReS10.

We show the presence of some systematic differences between the precipitation in CLARReS10-ERA40 and CLARReS10-R2. This difference does not parallel the difference in precipitation between the global reanalyses themselves: on average, the precipitation in ERA40 is less than that in R2, while the converse is true of CLARReS10-ERA40 and CLARReS10-R2. This apparent paradox could be explained by the difference in convective parameterization between the two global reanalyses and the difference in their low-level humidity fields. Since ERA40 contains more low-level moisture than R2, CLARReS10-ERA40 has more precipitation than CLARReS10-R2. However, despite the increased moisture in ERA40 compared to R2, it has a less efficient convective precipitation scheme and therefore rains less.

Even though our results suggest a slight advantage of CLARReS10-ERA40 over CLARReS10-R2 in their simulation of the spatial and temporal structure of precipitation, we prefer to refrain from making a definitive recommendation for use of one over the other. We feel that consideration of the range of regional model response to two different (yet arguably "perfect") boundary conditions provides an informative estimate of the regional level uncertainty.

Downscaling can reduce bias by capturing details of mesoscale features that are absent in the global reanalyses. However, it still suffers from weaknesses of the original reanalyses. We have highlighted the dependence of the dynamically downscaled precipitation on the boundary conditions.

We have demonstrated that the dynamical downscaling is capable of reducing precipitation biases at all time scales by capturing details of mesoscale features that are absent in the global reanalysis but are dictated by the large scale flow. However, an unavoidable weakness of such downscaling is that it is sensitive to inaccuracies or uncertainties of the original reanalysis

Given the degree of success in simulation of the characteristics of regional precipitation by the dynamic downscaling of global reanalyses over the Southeast United States and the cost-effectiveness of such downscaling, we strongly believe that this approach to regional reanalysis is a viable proxy for conventional reanalysis.

Nonetheless, high quality conventional reanalyses remain essential for the initialization of future extended re-forecasts.

Acknowledgements

The authors would like to express their gratitude to Dr. Kei Yoshimura for his assistance with the RSM model, Ms. Lauren Moeller for her help with data aggregation and storage, Ms. Kathy

Fearon for her editorial comments, Dr. David Sumner and three anonymous reviewers whose helpful comments and thoughtful critique of the manuscript have significantly improved it, and The Florida State University shared High-Performance Computing facility and staff for providing computational resources for this study.

The CPC Daily US Unified Precipitation and NCEP-DOE Reanalysis II data were provided by the NOAA/OAR/ESRL PSD, Boulder, Colorado, USA, from their web site at http://www.esrl.noaa.gov/psd/; PRISM monthly precipitation was provided by the PRISM Climate Group at Oregon State University from their website at http://www.prism.oregonstate.edu; ECMWF-ERA40 Reanalysis data were provided by the ECMWF from their data server at http://data.ecmwf.int. MERRA data were made available by the Global Modeling and Assimilation Office (GMAO) and the GES DISC.

Funding for this project was provided by grants from NOAA, USDA CREES and USGS.

References

Abbs, DJ and Physick, WL (1992): Sea-breeze observations and modeling: a review. Aust Met Mag 41:7-19

Betts, AK, Zhao M, Dirmeyer PA, and Beljaars ACM (2006): Comparison of ERA40 and NCEP/DOE near-surface data sets with other ISLSCP-II data sets. J Geoph Res 111, doi:10.1029/2006JD007174

Blanchard DO, López RE (1985) Spatial patterns of convection in South Florida. Mon Wea Rev 113:1282–1299

Byers HR, Rodebush HR (1948) Causes of thunderstorms of the Florida peninsula. J Meteorol 5:275-280

Castro CLS, Pielke RA, and Leoncini G (2005) Dynamical down-scaling: Assessment of value retained and added using the Regional Atmospheric Modeling System (RAMS). J Geophys Res 110, doi:10.1029/2004JD004721

Chan SC, Misra V (2010) A diagnosis of the 1979-2005 Extreme rainfall events in the southeastern United States with isentropic moisture tracing. Mon Wea Rev 138:1172-1185

Clark JS, Carpenter SR, Barber M, Collins S, Dobson A, Foley JA, Lodge DM, Pascual M, Pielke Jr. R, Pizer W, Pringle C, Reid WV, Rose KA, Sala O, Schlesinger WH, Wall DH, and Wear D (2001) Ecological forecasts: an emerging imperative. Science 293 (5530): 657-660, doi:10.1126/science.293.5530.657

Chou MD, Suarez MJ (1994) An efficient thermal infrared radiation parameterization for use in General Circulation Models. Technical Report Series on Global Modeling and Data Assimilation, National Aeronautical and Space Administration/TM-1994-104606, 3, 85 p

Chou MD, Lee KT (1996) Parameterizations for the absorption of solar radiation by water vapor and ozone. J Atmos Sci 53:1203–1208

Daly C, Neilson RP, Phillips DL (1994) A statistical-topographic model for mapping climatological precipitation over mountainous terrain. J Appl Meteorol 33:140-158.

Dickinson MJ, Bosart LF, Bracken WE, Hakim GJ, Schultz DM, Bedrick MA, Tyler KR (1997): The March 1993 Superstorm cyclogenesis: incipient phase synoptic- and convective-scale flow interaction and model performance. Mon Wea Rev 125:3041-3072

Ek MB, Mitchell KE, Lin Y, Rogers E, Grunmann P, Koren V, Gayno G, and Tarpley JD (2003) Implementation of Noah land surface model advances in the National Centers for Environmental Prediction operational mesoscale Eta model. J Geophys Res 108: D228851, doi:10.1029/2002JD003296

Higgins RW, Janowiak JE, and Yao Y-P (1996) A gridded hourly precipitation data base for the United States (1963-1993). NCEP/Climate Prediction Center Atlas 1, National Centers for Environmental Prediction, 46p

Hong S-Y, Pan H-L (1996) Nonlocal boundary layer vertical diffusion in a medium-range Forecast model. Mon Wea Rev 124:2322–2339

Huffman GJ, Adler RF, Bolvin DT, Gu G, Nelkin EJ, Bowman KP, Hong Y, Stocker EF, Wolff DB (2007) The TRMM multi-satellite precipitation analysis: quasi-global, multi-year, combined-sensor precipitation estimates at fine scale. J Hydrometeor, 8:38-55

Juang H-M, Kanamitsu M (1994) The NMC nested regional spectral model. Mon Wea Rev 122:3-26

Kalnay E et al. (1996) The NCEP/NCAR 40-year reanalysis project, Bull Amer Meteorol Soc 77:437-471.

Kanamaru H, Kanamitsu M (2007a) Scale-selective bias correction in a downscaling of global analysis using a regional model. Mon Wea Rev 135:334-350

Kanamaru H, Kanamitsu M (2007b) Fifty-seven-year reanalysis downscaling at 10km (CaRD10). Part II: Comparison with North American Regional Reanalysis. J Climate 20:5572-5592

Kanamitsu M, Ebisuzaki W, Woollen J, Yang S-K, Hnilo J, Fiorino M, and Potter GL (2002) NCEP-DOE AMIP-II reanalysis (R-2), Bull Amer Meteorol Soc, 83:1631–1643

Kanamitsu M, Kanamaru H (2007) Fifty-seven-year reanalysis downscaling at 10km (CaRD10). Part I: System detail and validation with observations. J Climate 20:5553-5571

Kocin KJ, Schumacher PN, Morales JR RF, Uccellini LW (1995) Overview of the 12-14 March 1993 Superstorm. Bull Amer Meteor Soc 76:165-182

Lim Y-K, Stefanova LB, Chan SC, Schubert SD, and O'Brien JJ, 2010: High-resolution subtropical summer precipitation derived from dynamical downscaling of the NCEP/DOE reanalysis: How much small-scale information is added by a regional model? Clim Dyn 35, doi: 10.1007/s00382-010-0891-2

Lin Y, Mitchell KE (2005) The NCEP stage II/IV hourly precipitation analyses: development and applications. Preprints 19th Conf on Hydrology, Amer Meteorol Soc, San Diego CA 9-13 Jan 2005

Messinger F, Dimego G, Kalnay E, Mitchell K, Shafran P, Ebisuzaki W, Jovic D, Woollen J, Rogers E, Berbery E, Ek M, Fan Y, Grumbine R, Higgins W, Li H, Lin Y, Manikin G, Parrish D, Shi W, 2006: North American Regional Reanalysis. Bull Amer Meteorol Soc 87:343-360

Michaels JP, Pielke R, McQueen JT, Sappington DE (1987) Composite climatology of Florida summer thunderstorms. Mon Wea Rev 115:2781-2791

Misra V, Moeller L, Stefanova L, Chan S, O'Brien JJ, Smith TJ III, Plant N (2010) The influence of Atlantic Warm Pool on Florida sea breeze. J Geoph Res (in review).

Pan H-L, Mahrt L (1987) Interaction between soil hydrology and boundary layer developments. Boundary-Layer Meteorol 38:185-202

Pan H-L, Wu W-S (1994) Implementing a mass-flux convective parameterization package for the NMC Medium Range Forecast Model. Preprints, 10th Conf. on Numerical Weather Prediction, Portland, OR, Amer Meteorol Soc, pp96–98.

Rahbek C, Graves GR (2001) Multiscale assessment of patterns of avian richness. PNAS 98 (8): 4534-4539, doi: 10.1073/pnas.071034898

Saha S et al. (2010) The NCEP climate forecast system reanalysis. Bull Amer Meteorol Soc, doi: 10.1175/2010BAMS3001.1

Schwarts BE, Bosart L (1979) The diurnal variability of Florida rainfall. Mon Wea Rev 107:1535-1545

Shukla J, Hagedorn R, Hoskins B, Kinter J, Marotzke J, Miller M, Palmer T, Slingo J (2009): Revolution in climate prediction is both possible and necessary. A declaration at the world modelling summit for climate prediction. Bull Amer Meteorol Soc, doi: 10.1175/2008BAMS 2759.1

von Storch H, Langenberg H, Feser F (2000) A spectral nudging technique for dynamical downscaling purposes. Mon Wea Rev 128:3664–3673

Slingo JM (1987) The development and verification of a cloud prediction scheme for the ECMWF model. Q J Roy Meteorol Soc 113:899–927

Smith TM, Reynolds RW, Peterson TC, Lawrimore J (2008) Improvements to NOAA's historical merged land-ocean surface temperature analysis (1880-2006). J Climate 21:2283-2296

Stefanova L, Misra V, O'Brien JJ, Chassignet EP, Hameed S (2011) Hindcast skill and predictability for precipitation and two-meter air temperature anomalies in global circulation models over the Southeast United States. Clim Dyn 36, doi: 10.1007/s00382-010-0988-7

Uppala SM et al (2006) The ERA40 re-analysis. Q J Roy Meteorol Soc, DOI 10.1256/qj.04.176

Warner TT, Peterson RA, Treadon RE (1997) Tutorial on lateral boundary conditions as a basic and potentially serious limitation to regional numerical weather prediction. Bull Amer Meteorol Soc 78:2599-2618

Winsberg MD (2003) Florida Weather. University Press of Florida, 218p

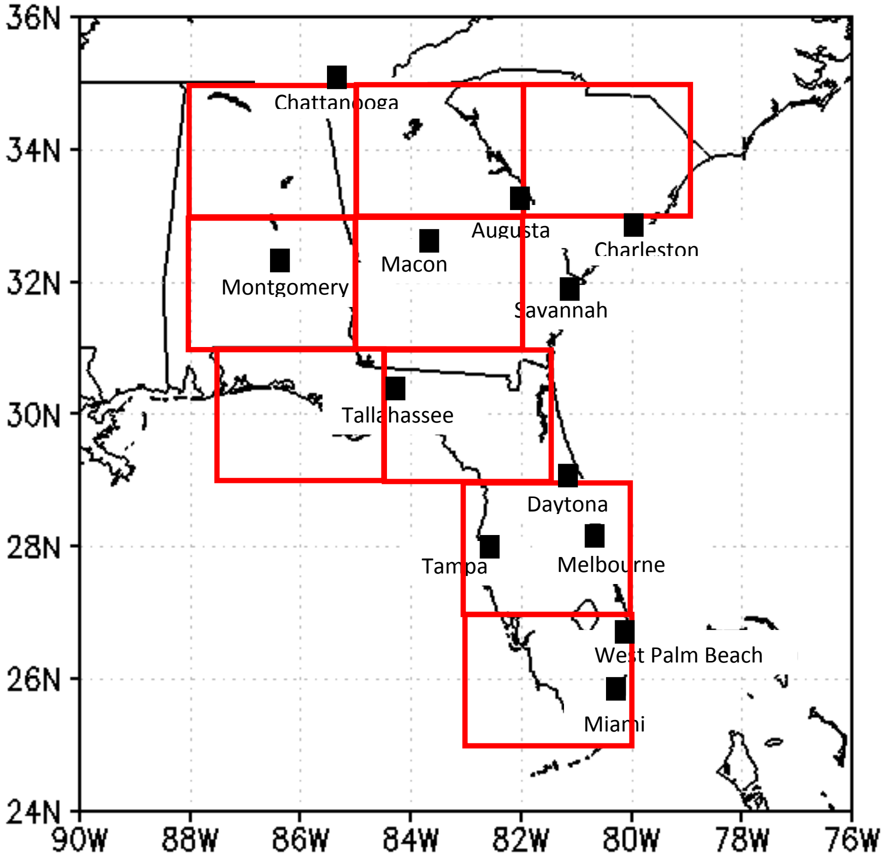

Fig. 1 Model domain. Red boxes indicate nine 3^{o}-by-2^{o} regions used for area-averaging. Labeled squares show the stations whose observations of hourly precipitation were used for diurnal cycle assessments

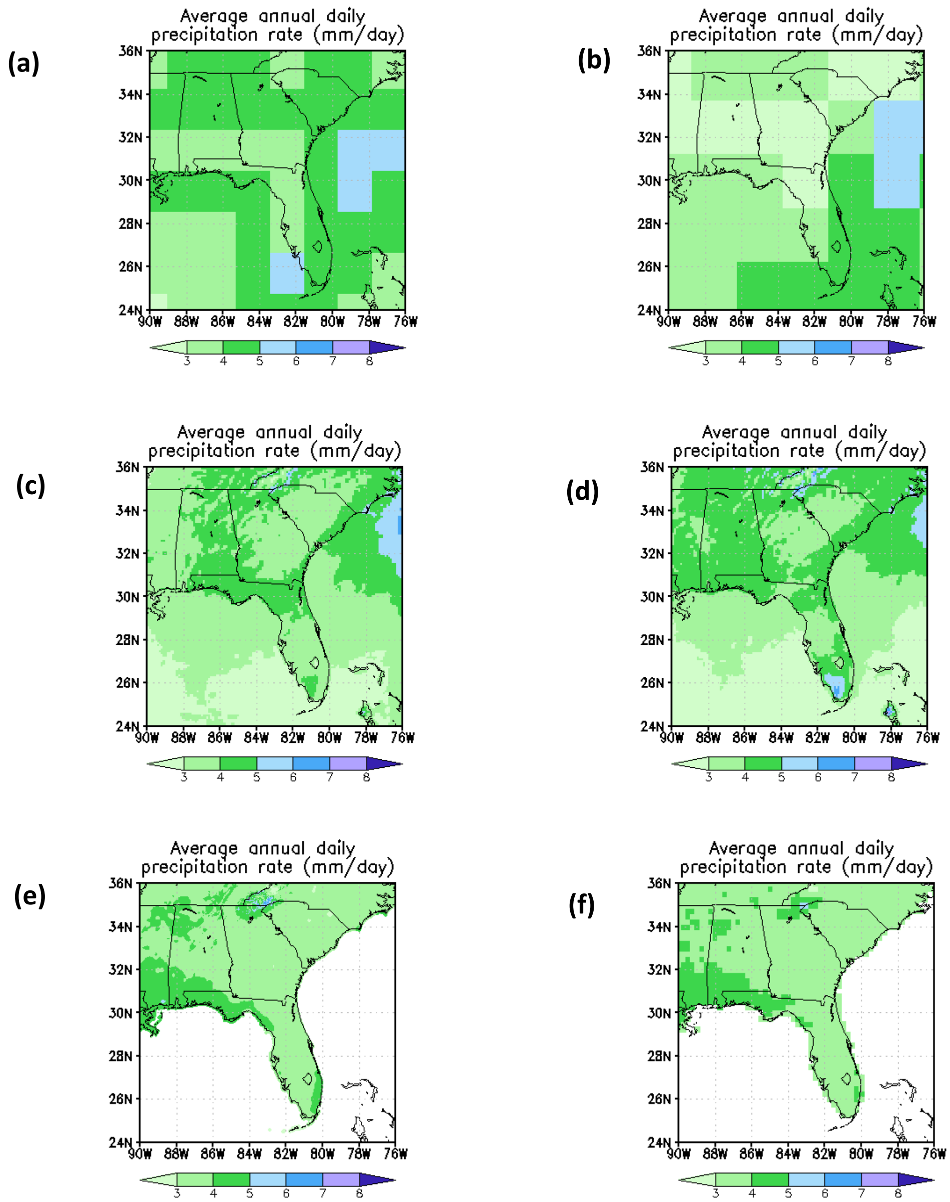

Fig. 2 Average annual precipitation rate (mm day^{-1}) from (a) R2, (b) ERA40, (c) CLARReS10-R2, (d) CLARReS10-ERA40, (e) CPC Daily US Unified Precipitation, and (f) PRISM

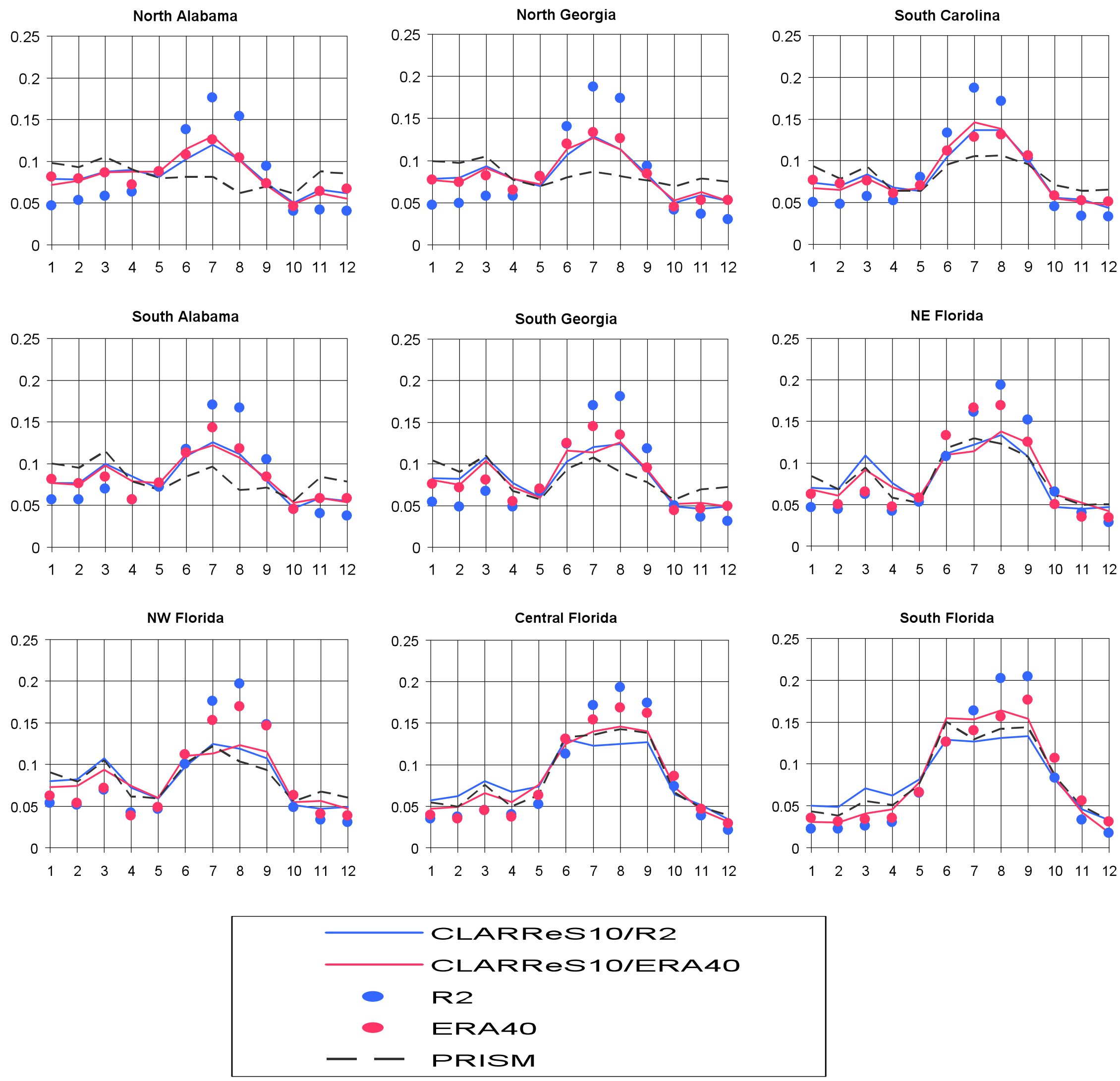

Fig. 3 Fractional contribution of calendar month (1-12) to the annual total, averaged over the boxes shown in Fig. 1

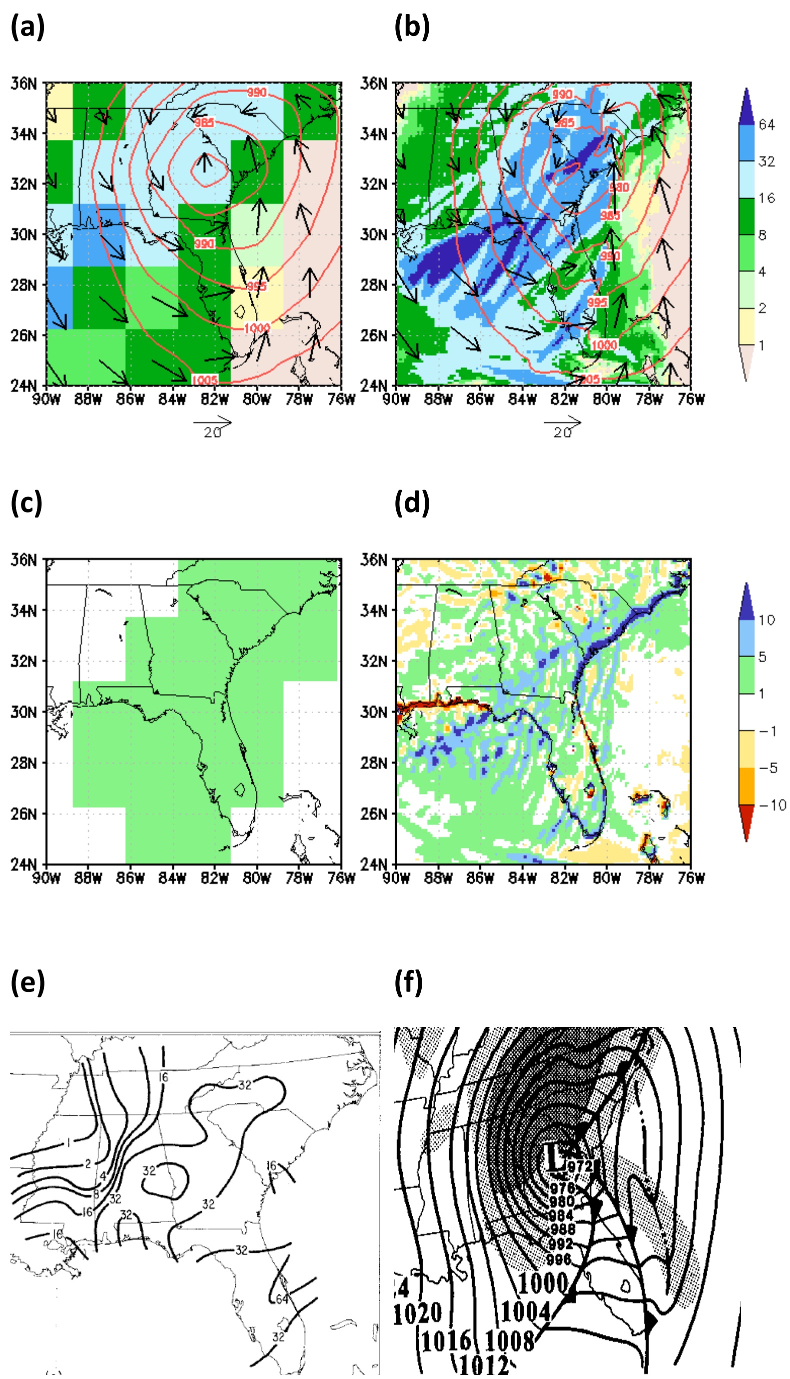

Fig.4 “Storm of the century”, 12z 13 March 1993: (a) ERA40 12-hour accumulated precipitation (shading, mm), instantaneous mean sea level pressure (contours, mb), and surface winds (arrows); (b) as in (a) but from CLARReS10-ERA40; arrows drawn once every 25 grid points; (c) ERA40 12-hour average convergence (units $10^{-5}s^{-1}$); (d) as in (c) but from CLARReS10-ERA40; (e) observed 12-hour accumulated precipitation (from Dickinson et al 1997); (f) observed instantaneous surface pressure and fronts (from Kocin et al 1995)

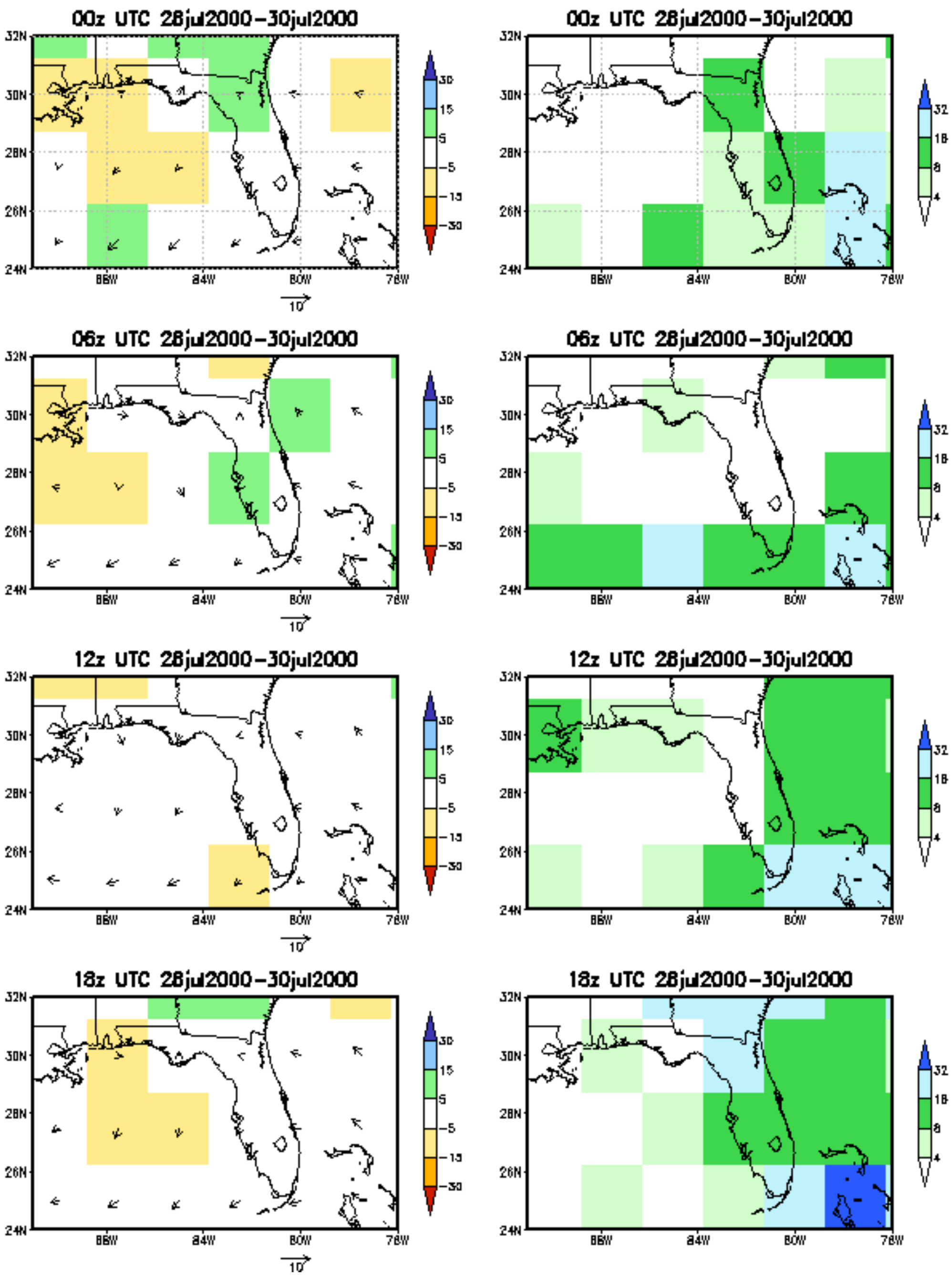

Fig. 5 ERA40 composite diurnal cycle for 28-30 July 1992. Left: surface convergence (units of 10^{-6} s^{-1}) and surface winds (m s^{-1}). Right: 6-hour average precipitation rate (mm day^{-1})

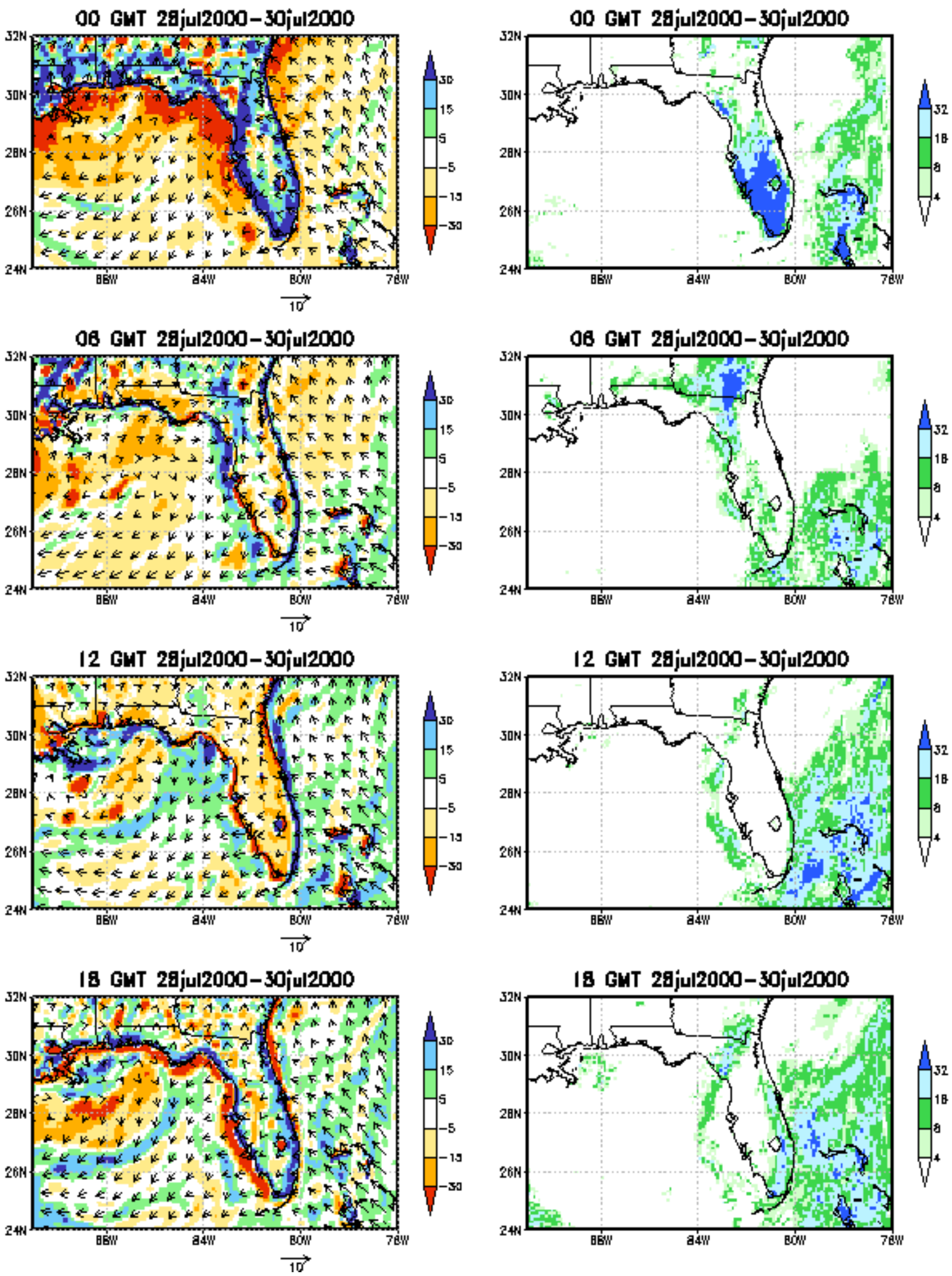

Fig. 6 As in Fig 6 but for CLARReS10-ERA40

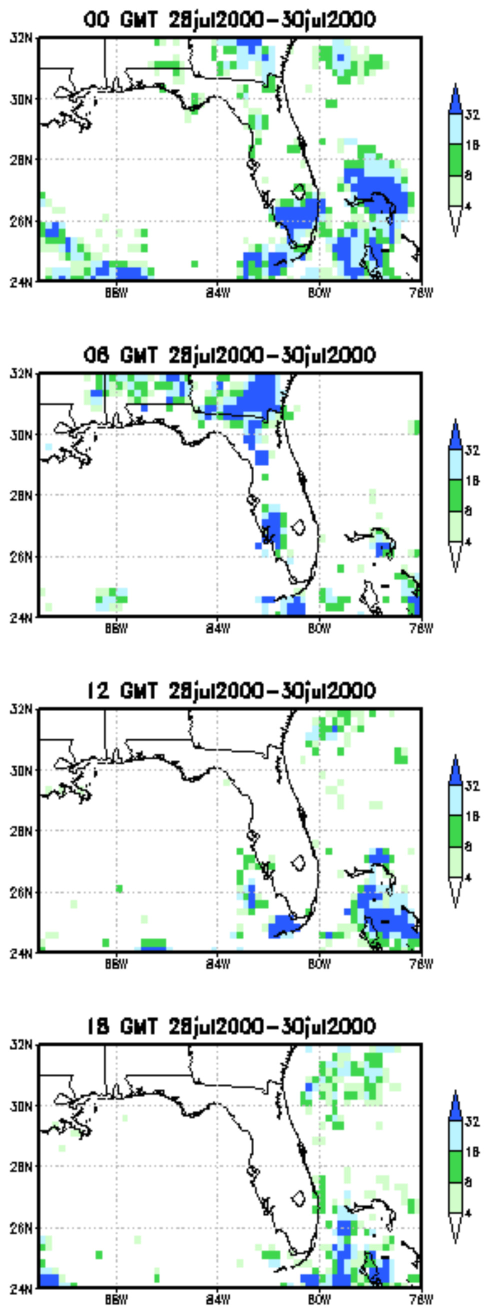

Fig. 7 Observed composite diurnal cycle of precipitation rates (mm day^{-1}) for 28-30 July 2000, 6-hour averages, derived from the TRMM 3B42 3-hourly product

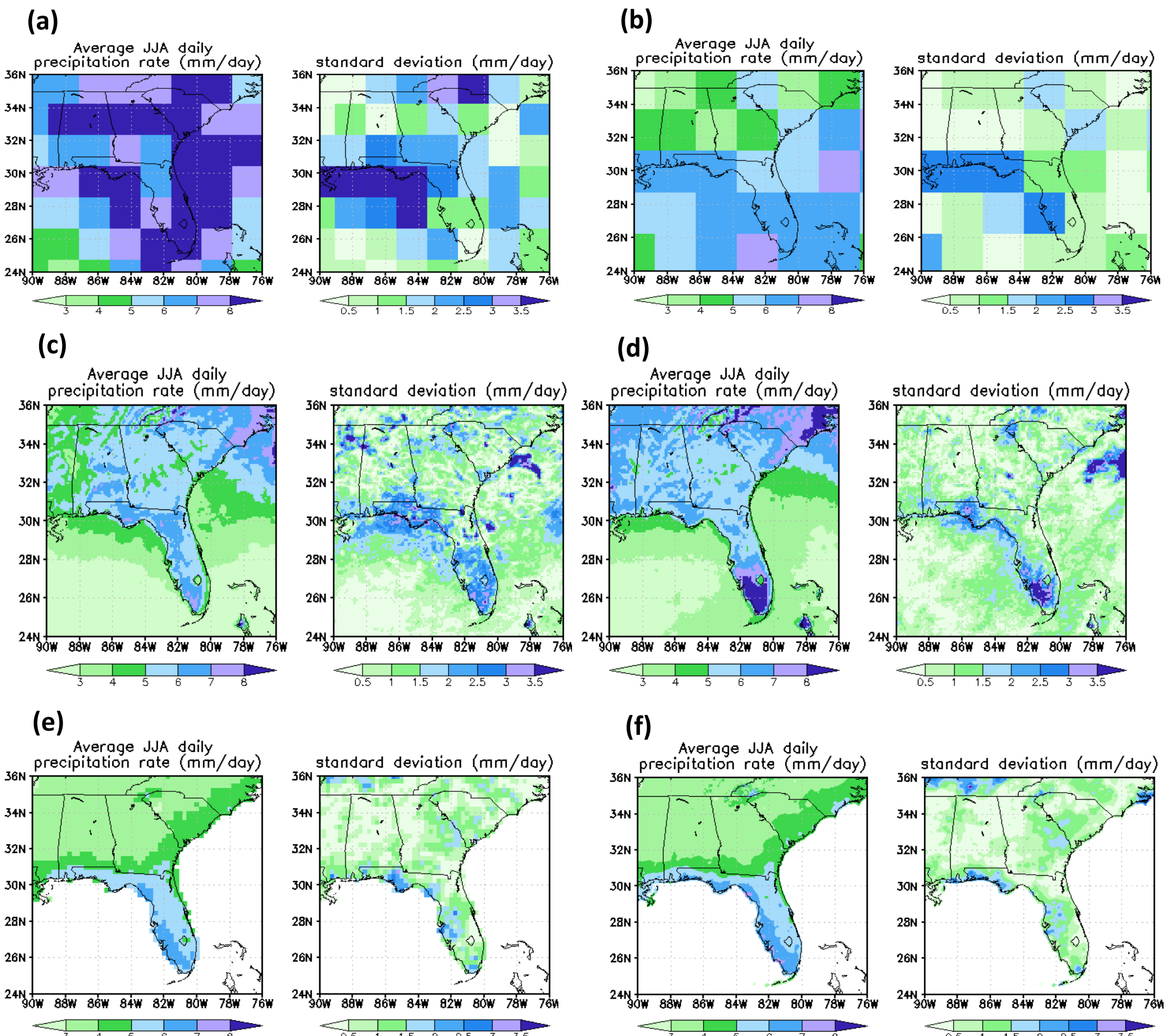

Fig. 8 Average summer (JJA) precipitation rate (mm day^{-1}) and standard deviation from (a) R2, (b) ERA40, (c) CLARReS10-R2, (d) CLARReS10-ERA40, (e) CPC Daily US Unified Precipitation, and (f) PRISM

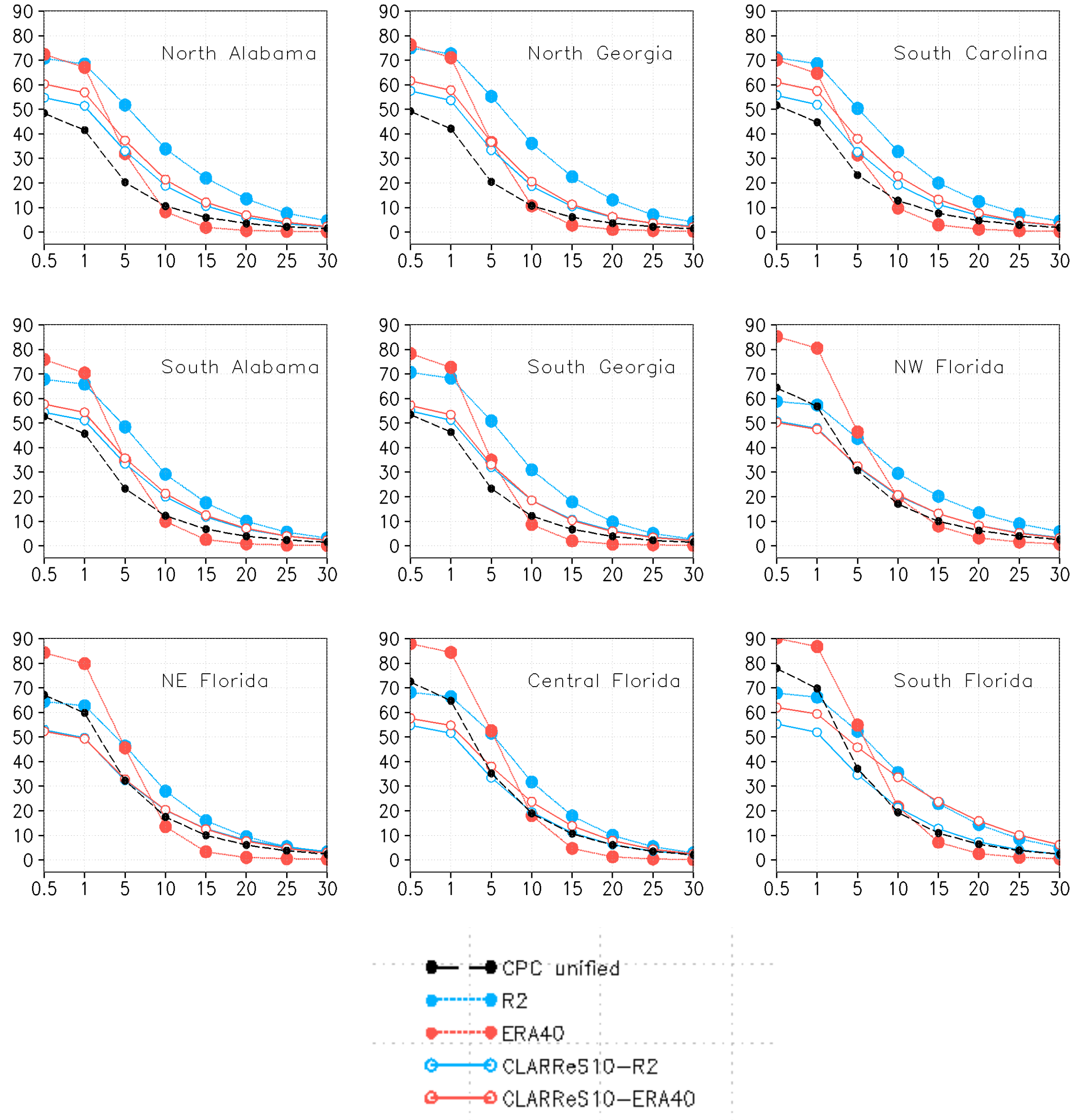

Fig. 9 Area-averaged percentage of JJA days with precipitation exceeding the threshold indicated on the x-axis (mm). The area averaging is performed over the boxes defined in Fig. 1

(a) **(b)**

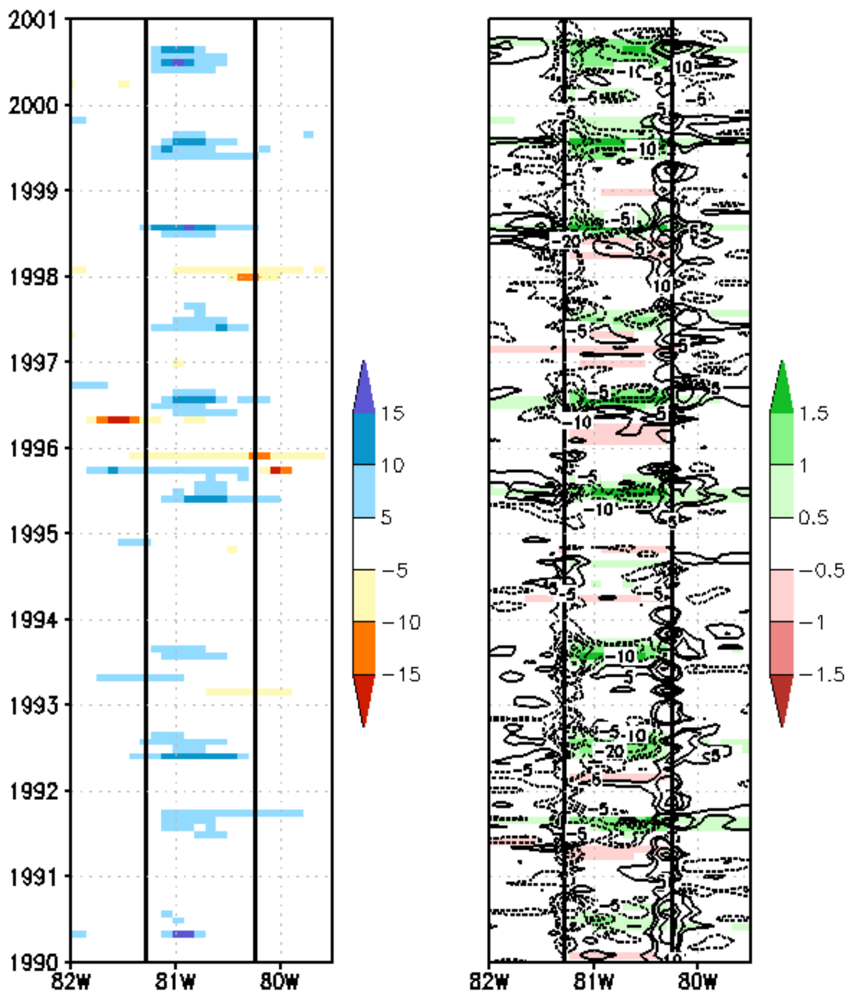

Fig. 10 Time-longitude cross-section from January 1990 through January 2001 at 25.5N of monthly mean difference in (a) precipitation (units mm day^{-1}) and (b) surface specific humidity (shading; units g kg^{-1}) and surface moisture convergence (contours; units 10^{-5} g kg^{-1} s^{-1}, contour interval 5, zero contour omitted) of CLARReS10-ERA40 minus CLARReS10-R2. Bold lines indicate the land-ocean boundary

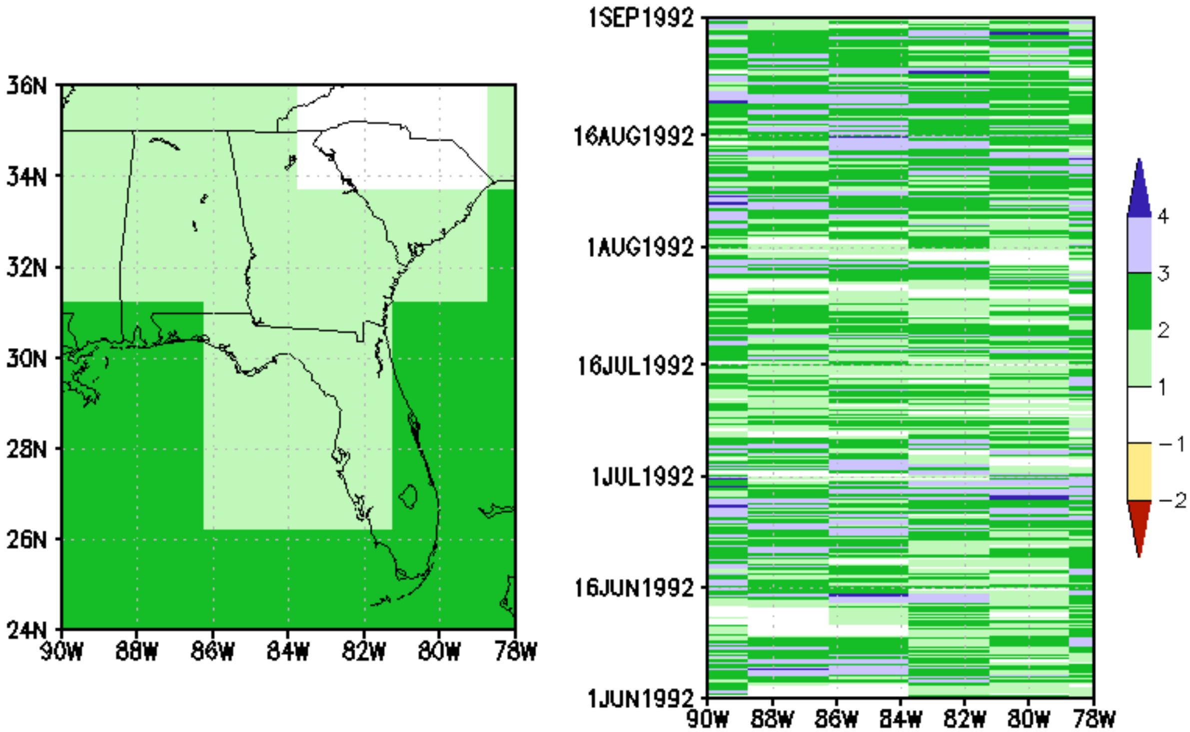

Fig. 11 Low-level (1000-850mb) JJA 1992 specific humidity difference of ERA40 minus R2 (units of g kg^{-1}). Left: averaged over the season; right: time-longitude cross-section at 25N

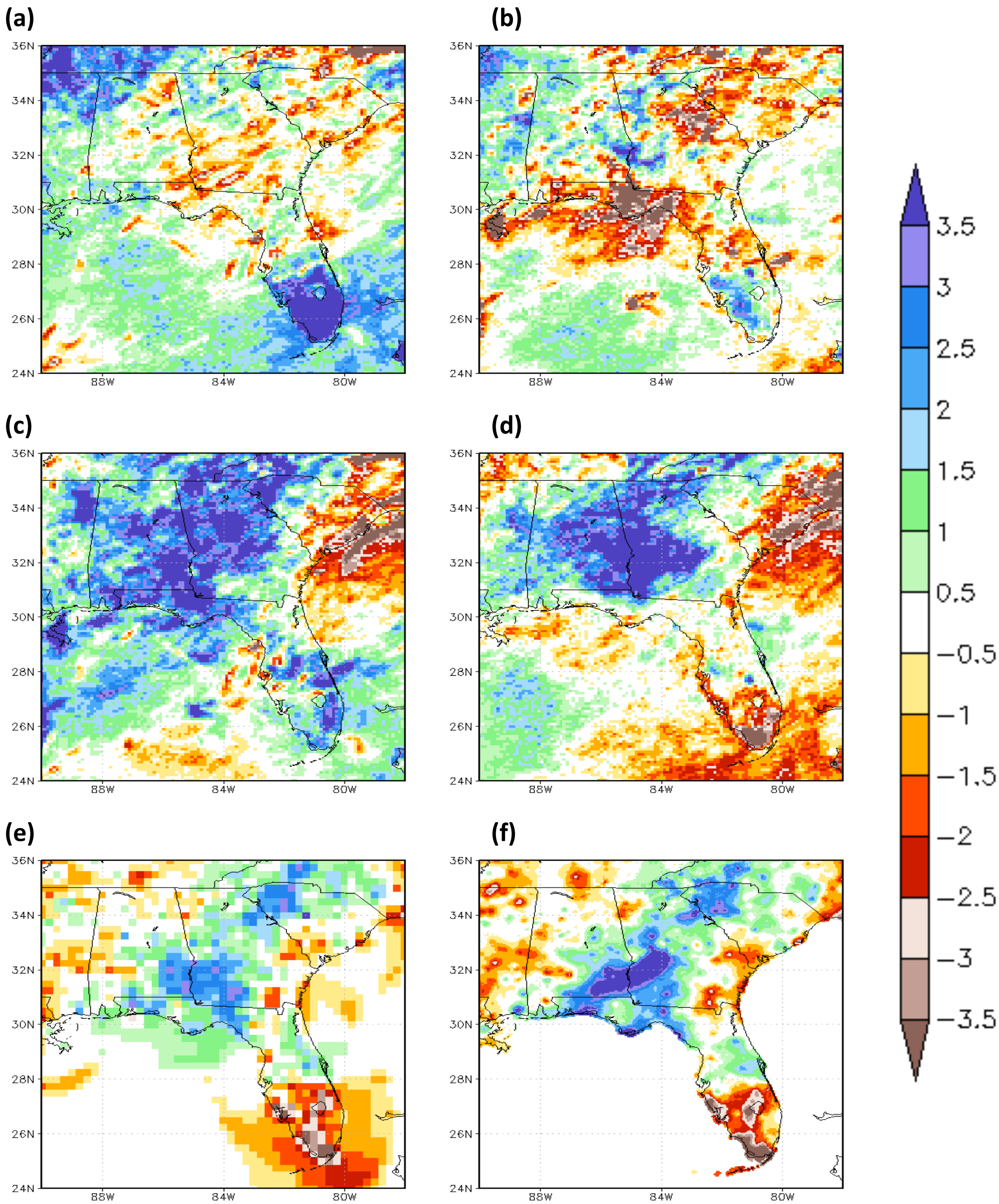

Fig. 12 JJA precipitation difference in mm day^{-1} for (a) CLARReS10-ERA40 minus CLARReS10-R2 for 1992; (b) CLARReS10-ERA40 minus CLARReS10-R2 for 1994; (c) CLARReS10-R2, 1994 minus 1992; (d) CLARReS10-ERA40, 1994 minus 1992; (d) PRISM, 1994 minus 1992; (e) CPC Daily US Unified Precipitation

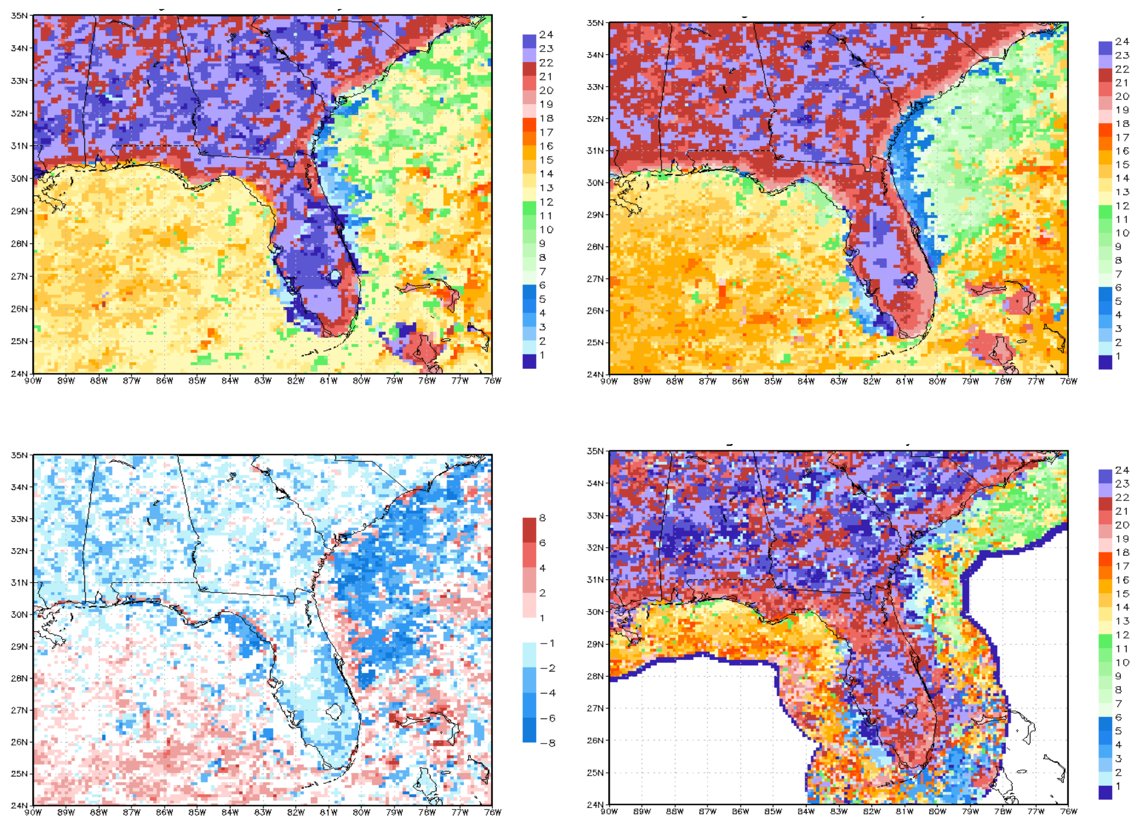

Fig. 13 Average timing of 1979-2001 JJA diurnal maximum (GMT) between CLARReS10-R2 (top left) and CLARReS10-ERA40 (top right); the difference in timing (CLARReS10-R2 minus CLARReS10-ERA40) in hours (bottom left); and the average timing of JJA diurnal maximum from NCEP/EMC multi-sensor estimate for 2004-2009 (bottom right)

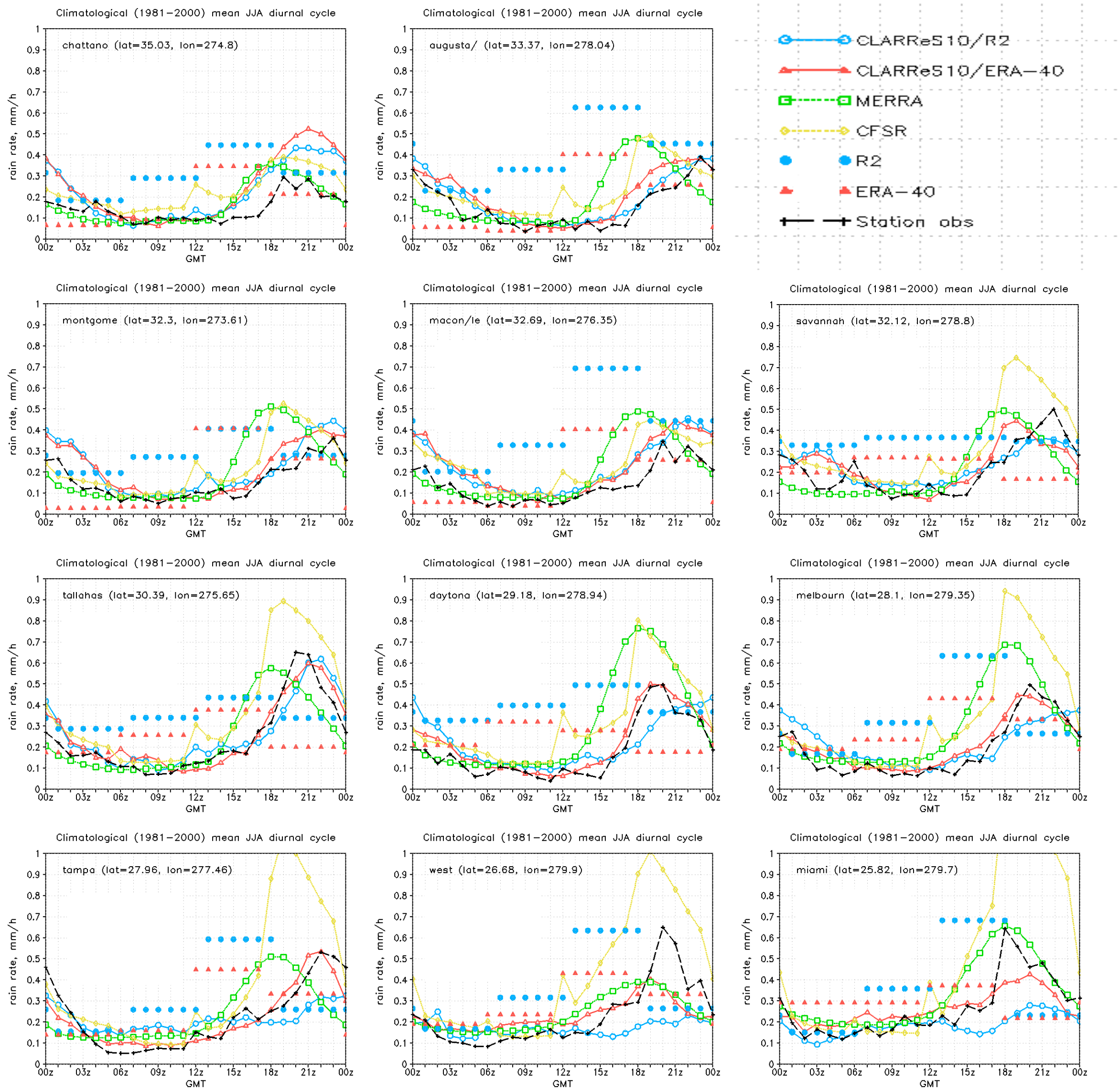

Fig. 14 JJA diurnal cycle of precipitation for several stations from the two global reanalyses (R2 and ERA40), their regionally downscaled counterparts (CLARReS10-R2 and CLARReS10-ERA40), MERRA, CFSR, and station data, as a function of GMT; EDT=GMT-4. The stations, going from left to right and from the top down are: Chattanooga TN, Augusta GA, Montgomery AL, Macon GA, Savannah GA, Tallahassee FL, Daytona FL, Melbourne FL, Tampa FL, West Palm Beach FL, and Miami FL

	Feature	Reference
1	Dynamics: hydrostatic primitive equations with spectrally transformed onto Fourier basis functions	Juang and Kanamitsu (1994)
2	10-km horizontal resolution; 28 vertical layers; 4-min resolution orography	Kanamaru and Kanamitsu (2007)
3	Planetary boundary layer processes	Hong and Pan (1996)
4	Shortwave and longwave radiation	Chou and Lee (1996); Chou and Suarez (1994)
3	Shallow convection	Slingo (1987)
4	Deep convection: Simplified Arakawa-Schubert Scheme	Pan and Wu (1995)
5	Boundary forcing: scale selective bias correction	Kanamaru and Kanamitsu (2007)
6	Land surface: Noah; 4 soil layers	Ek et al. (2003)

Table 1 RSM configuration and main features